On The Diffusion of Sticky Particles in 1-D

Joshua DM Hellier[*] and Graeme J Ackland[†]
SUPA, School of Physics and Astronomy, University of Edinburgh,
Mayfield Road, Edinburgh EH9 3JZ, United Kingdom
(Dated: September 11, 2018)

The 1D Ising model is the simplest Hamiltonian-based model in statistical mechanics. The simplest interacting particle process is the Symmetric Exclusion Process (SEP), a 1D lattice gas of particles that hop symmetrically and cannot overlap. Combining the two gives a model for sticky particle diffusion, SPM, which is described here. SPM dynamics are based on SEP with short-range interaction, allowing flow due to non-equilibrium boundary conditions. We prove that SPM is also a detailed-balance respecting, particle-conserving, Monte Carlo description of the Ising model. Neither the Ising model nor SEP have a phase transition in 1D, but the SPM exhibits a non-equilibrium transition from a diffusing to a blocked state as stickiness increases. We present a fully non-linear, analytic, mean-field solution, which has a crossover from a positive to a negative diffusion constant. Simulations in the positive-diffusion region agree with the analytics. The negative diffusion constant in fact indicates a breakdown of the mean-field approximation, with close to zero flow and breaking into a two-phase mixture, and thus the mean field theory successfully predicts its own demise. The simplicity of the model suggests a wide range of possible applications.

I. INTRODUCTION

Lattice gases are a ubiquitous tool for modeling complex systems from biology to traffic [1–7]. Analytically solvable cases involve non-interacting or excluding particles [8–13], but in any real system of interest the moving objects interact. Many models tackle the situation where the diffusing object interact with the substrate, but despite the clear application-relevance there is surprisingly little work considering interactions between the moving particles themselves. One reason for this is that the interactions introduce nonlinearities in analytical models, which makes them challenging to solve, at least outside of limits in which they can be linearized. This is unfortunate because it is precisely these nonlinearities which introduce interesting behaviors such as discontinuities at the oxide-metal interface or diffusion instability [14, 15].

Another feature of previous models is that the flow is driven by either asymmetry in the dynamics (e.g. ASEP) or an external field which permeates the system (e.g. KLS). In either case, the particles always see a local asymmetry. However in many systems the flow is driven by a pressure or chemical potential difference applied at the boundaries, so that any local asymmetry arises from self-organization. This situation is addressed here.

In this paper we will investigate what we believe ito be the simplest such one-dimensional model, the "Sticky Particle Model" or SPM, specified in the top left inset of Fig. 1, which contains such an interaction, and we will explore the impact this has on particle behavior, in particular when observed in the large-scale limit. One might contrast this approach (making a simple microscopic model and trying to learn from it about large-scale

———————
[*] J.D.M.Hellier@sms.ed.ac.uk
[†] G.J.Ackland@ed.ac.uk

FIG. 1.   White circles indicate particles, dark circles indicate empty sites (vacancies). Particles randomly move into adjacent vacancies with rate 1 (having rescaled time for notational convenience), unless there is a particle behind the position they're moving from, in which case they move with rate λ; the state of the site next to the position the particle is moving into is irrelevant.
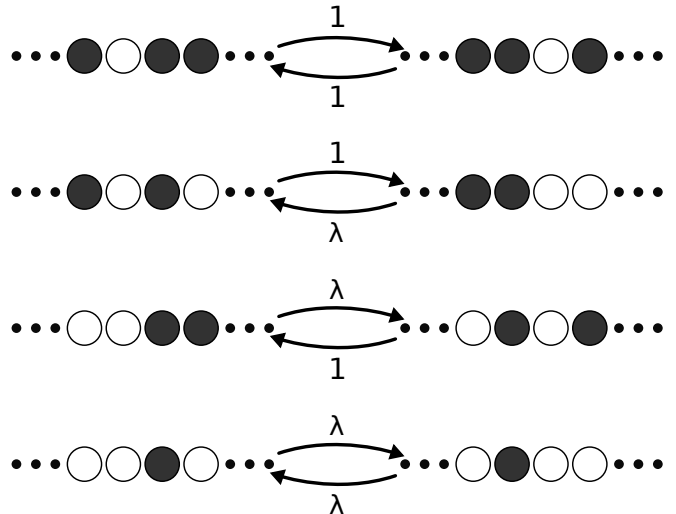
interface growth) with approaches such as the KPZ equation [16–18] (where one analyses the extreme large-scale dynamics using universality classes).

II. THE STICKY PARTICLE MODEL

The SPM is an excluded-particle model in which adjacent particles separate with rate λ and single particles move at rate 1.

It differs from the symmetric exclusion process [19–24]; in that particles "unstick" with rate λ instead of their

normal hopping rate, 1. Low λ corresponds to sticky particles, high λ to repelling particles. It could be regarded as a version of the KLS model [25–27] in 1-dimension without an applied field, which is itself similar to the dynamics used to analyze the Ising model by Kawasaki [28]. The KLS model has a field which introduces an asymmetry which drives a flow. It is tacitly assumed that this field is required for the nontrivial flow behavior seen in the model, so the simpler symmetric model has received less attention.

A. Detailed Balance Proof

The SPM is intended to study flow, so it is *defined* by the hopping rates. In Fig. 1 we show all the possible transitions which may occur between local configurations.

Assume that the system is now on a ring, with L lattice sites and N particles. Let us label possible system configurations by ξ and let the number of adjacencies (or "bonds") between particles be $b(\xi)$. Now for our ansatz, assume that the probability of the system being in state ξ is $\lambda^{-b(\xi)}$. In the top and bottom diagrams of Fig. 1 we can see that the number of bonds on both sides is the same, as are the transition rates back and forth; thus our ansatz holds for these states, as it predicts the probabilities of the left and right configurations are the same. The middle two diagrams are equivalent; in the upper diagram a bond is formed going left to right and then broken going right to left, so the probability of being in the left state is λ times that of being in the right state. This is again in agreement with the detailed balance criterion. As these are the only types of transition that may occur on a ring, we have proven that the closed system obeys detailed balance, with an energy proportional to $b(\xi) \ln \lambda$

B. Equivalence to Ising Model at Equilibrium

Since the model obeys detailed balance, there must be an associated Hamiltonian. This is simply proportional to the number of particles stuck together:

$$H = q \sum_i p_i p_{i+1} = q b(\xi) \tag{1}$$

where p_i is 1 for a particle or zero for and empty site. A simple transformation $s_i = 2p_i - 1$ shows this to be equivalent to the Ising Hamiltonian

$$H = q \sum_i \left[\frac{1}{4} s_i s_{i+1} + \left(\frac{1}{2} s_i + \frac{1}{4} \right) \right] \tag{2}$$

The contribution from the final term is constant, as only hopping moves are allowed so $\sum s_i$ is constant. So at equilibrium the SPM samples the 1D Ising model with fixed magnetization, a fact which was used to validate the codes. Compatibility between the detailed balance condition, the standard Boltzmann distribution at temperature T and our defined rates requires that $q = k_B T \ln \lambda$.

III. TRANSITION RATE MATRIX CALCULATIONS

The SPM, just like the KLS model and ASEP, can exhibit flow. In this paper we will be principally concerned with the computation of the flow that results when an SPM system of L sites is connected to (unequal) particle reservoirs at either end.

It is actually possible to "analytically" solve the SPM on a finite domain with fixed boundary densities by analyzing the transition rate matrix which represents that system. To do this, we wrote a Python code, in which specific configurations of a system of length $L + 4$ are represented by strings of binary numbers. For example, the configuration "00101011" corresponds to a system with $L = 4$ where there is a particle in sites with a "1" and a vacancy in sites with a "0". As there is a clear correspondence between binary strings and positive integers, in our code we loop over the configurations; in each configuration, we can loop over the particles, see which moves they can make and with what rates, and which configurations these moves would take us to. Doing this allows us to add entries to a sparse matrix representation of the SPM with boundary conditions.

There are a pair of additional sites at each boundary in order to simulate the particle reservoirs, hence why the overall system size is $L + 4$. We do this by allowing particles in these boundary layers to rapidly pop in and out of existence, with rates such that the mean occupation should be the desired boundary density. The choice of how to achieve this is not unique, but in our computations the rate at which particles appear in empty spaces at the left boundary is

$$C_0 (1 + \lambda) \sqrt{\lambda \frac{\rho_0}{1 - \rho_0}}, \tag{3}$$

and the rate at which particles disappear is

$$C_0 (1 + \lambda) \sqrt{\lambda \frac{1 - \rho_0}{\rho_0}}. \tag{4}$$

In isolation, the above rates would ensure that the average occupation was always ρ_0. In our overall SPM system, we attempt to ensure that both of these rates are larger than, or at the very least not smaller than, the other rates in the system (1 and λ); this should ensure that the occupation of the boundary sites is always approximately ρ_0, regardless of what is happening internally. Thus, C_0 is chosen to be quite large, and the λ-dependence exists primarily in order to ensure that λ does not dominate the boundary rates when it becomes large. An analogous set of rates are used at the right boundary. It is worth noting that with the addition

of these boundary conditions, the model as a whole no longer obeys detailed balance, even though the bulk still does in terms of local behavior.

Once we have built the correct transition rate matrix, we then use the Python routine `scipy.sparse.linalg.eigs` to find the eigenvector and associated eigenvalue with the largest real part. As it is a matrix whose exponential corresponds to an irreducible stochastic matrix, it is guaranteed to have a unique zero eigenvalue, corresponding to the long-term steady state. All other eigenvalues have negative real part, and are either purely real or arranged into conjugate pairs (as the matrix is real). The stationary state contains most of the key information we desire about the system's behavior during steady flow, including the flow rate and particle density profile, which may be accessed by the application of occupation and current operators (constructed along with the transition rate matrix). The next least-negative eigenpairs dominate the approach to equilibrium, and determine the timescale over which it is achieved.
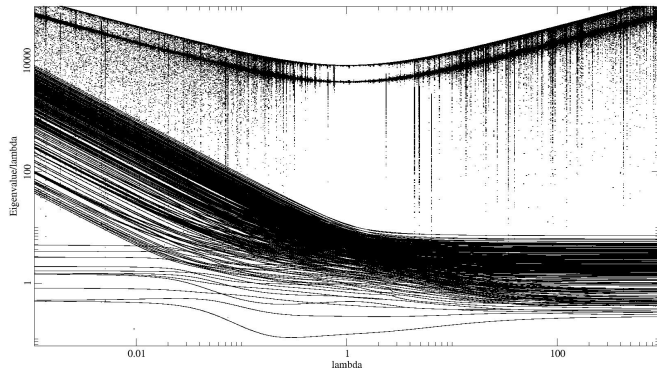

FIG. 2. The moduli of the 1024 most positive eigenvalues of the the transition rate matrix for the SPM for a system of size 8 as a function of λ, computed using sparse numerical linear algebra. We have divided the modulus by λ before plotting, as this makes the $\mathcal{O}(\lambda)$ trend in the low-lying eigenvalues much more apparent; as these eigenvalues correspond to the decay rates of the dominant unsteady states in the system, this implies that the time taken for a simulated system to relax to its equilibrium state scales inversely proportional with λ, which helps explain the poor convergence of our Monte Carlo simulations in that regime. Observe also that for intermediate λ eigenvalues often merge or cross; this implies the existence of rich behavior, and suggests that finding a full analytic solution to for this model might be difficult.

The near-zero eigenspectrum of the transition rate operator, and its dependence upon λ for fixed boundary conditions, is extremely interesting in its own right, as shown in Fig. 2. The structure is rich, with eigenvalues frequently crossing over each other, as well the appearance and disappearance of "bands", similar to those which one would see in electronic structure theory. Repeat calculations show that large changes in C_0 cause very small changes in the low-lying eigenspectrum of the

transition rate matrix, so in this sense the parameter is "irrelevant", as desired. It does have quite an impact on the group of eigenvalues of larger magnitude, which form a u-shape towards the top of Fig. 2, suggesting that the group is associated with rapid changes in configuration due to the blinking effect at the boundaries. One of the most notable features of the eigenspectrum is the presence of a relatively small number of low-lying eigenvalues which seem to split off from the main sequence as λ becomes much smaller than 1; they have $\mathcal{O}(\lambda)$ scaling, whilst the main sequence has $\mathcal{O}(1)$ scaling. This split may coincide with, and be related to, a suspected transition, which we will discuss in more detail in Section IV C. System size variations suggest that the number of eigenvalues which belong to this grouping scale as $\mathcal{O}(2^{\sim 0.8L})$, and so slower than the total number of eigenvalues, 2^{L+4}, suggesting that this "band" is unusually thin.

Unfortunately the the space complexity of the sparse transition rate matrix scales as $\mathcal{O}(2^L L)$ (although the matrix density scales as $\mathcal{O}(2^{-L} L)$, so the sparse format is definitely worth it). The overall time complexity for this process is $\mathcal{O}(2^{2L} L)$, although many parts of the calculation could be parallelized efficiently if so desired. In spite of this, we have managed to compute properties such as the steady-state flow rate for systems with sizes as large as 10 internal lattice sites, which are large enough to produce consistent outputs comparable to our other methods, whilst being computationally cheap enough to compute en masse.

In addition, we have also performed Monte Carlo simulations using a couple of different methods, which allows us to better probe the large-system regime. In the simulations and "analytics", we can vary ρ_0, ρ_L and λ to address three questions: how does λ affect the flow, how does the particle current depend on the driving force $(\rho_0 - \rho_L)/L$, and how does the density of particles in the system vary?

IV. SIMULATIONS

In the SPM the bulk dynamics are perfectly symmetric, and flow is driven by setting ρ at the boundaries, with the system self-organizing to give the steady-state density. The flow rate, Hamiltonian energy and particle density of the system are fully determined by (ρ_0, ρ_L) and the unsticking rate λ; this has been so far confirmed in our "analytics" by the existence and uniqueness of the steady flow state in every instance we have tried.

We can simulate flow in a bounded domain using Monte Carlo methods. In the bulk, the transition rates are simply those described in Fig. 1. At the boundaries we used a similar two-layer boundary trick to that described in Sec.III, only this time the particle appearance and disappearance have rates

$$\sqrt{\lambda \frac{\rho_0}{1 - \rho_0}}, \tag{5}$$

and

$$\sqrt{\lambda \frac{1-\rho_0}{\rho_0}}. \tag{6}$$

respectively. Whilst it would be nice for these rates to be large in order to force the boundaries to maintain the correct density more accurately, we choose to simply keep them proportional to the geometric mean of 1 and λ, otherwise they tend to either happen too rarely or far too frequently, causing the KMC algorithm to be inefficient.

We chose to calculate primarily by using the `KMCLib`[29] package, which implements the Kinetic Monte Carlo algorithm (essentially the same as the Gillespie algorithm[30–32]) on lattice systems. The codes used are kept here [33]. Independent of the KMCLib code, we wrote a simple Metropolis-Hastings algorithm [34] which randomly selects single particle hops; this is more efficient than using KMC for values of λ which are relatively close to 1 as the algorithm is simple and the acceptance rate is relatively high, so we can generate better statistics using this method in that regime. We calculate the flow from the number of particles entering and leaving the system at the boundaries. Since the model is defined in terms of *rates*, the flow in "particles per unit time" is a well defined quantity.

Using KMClib we studied systems of length 64 (lengths 32, 128 and 256 give similar results as shown in Fig. 6.), running them for 400000 Gillespie steps for equilibration followed by 10000 measurement runs of 1000 steps interspersed with relaxation runs of 16000 steps. This way we could gather statistics about flow rates and densities in a well-equilibrated system. Specifically, we generate a pool of 10000 samples of flow rate and density, from which we can calculate estimates of the descriptive statistics of both quantities. These calculations, in which we held the boundary densities constant whilst varying λ, were repeated using Metropolis-Hastings for a length 100 system, and we have transition rate matrix currents for a system of length 10. These are plotted on both logarithmic and linear axes in Fig. 3. respectively.

A.   Diffusion Coefficient

We compare an MFT prediction (see V) and the KMC numerical results for the diffusion constant in Fig. 11. We see that MFT and simulation agree well for low stickiness, and both show the symmetry about $\rho_M = \frac{2}{3}$. For high stickiness, where the MFT prediction gives negative diffusion constant, we actually see low positive values for the current. It should be noted that the MFT assumes that $\rho = \rho_M$ throughout, whereas in the simulations ρ tends to be much higher.
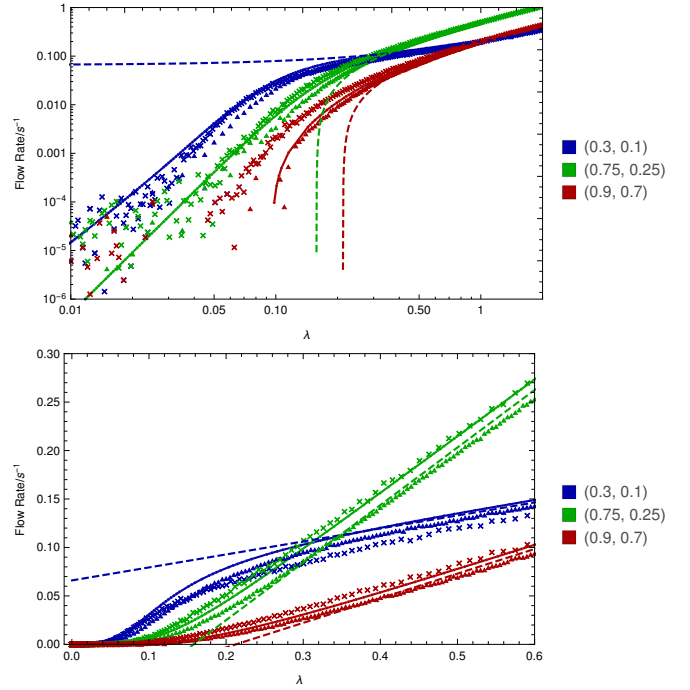

FIG. 3. The variation of (normalized) flow rate with λ in the SPM with fixed boundary densities, on both logarithmic and linear scales. Crosses indicate results from the KMC simulations, triangles those from the traditional Metropolis-Hastings simulations and the joined circles the current observed by finding the least dominant eigenvector in the transition rate matrix. The dashed lines are the corresponding MFT prediction for the current, and color indicates the boundary conditions used. The flow rate is normalized in the sense that it has been multiplied by the system size, so that we can easily compare between different system sizes. We do have estimates of the standard error in the flow rate, but as we have an abundance of data points we feel that the spread of the points on the graph illustrates it well enough.
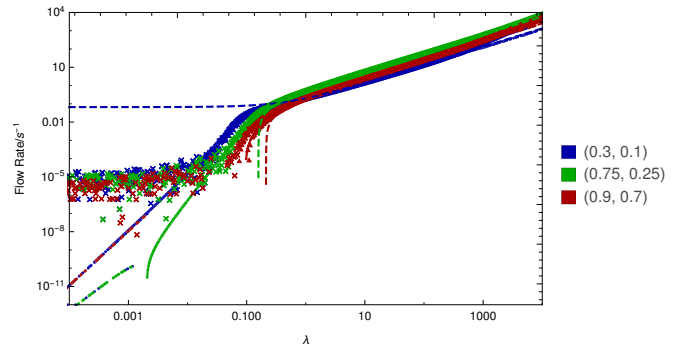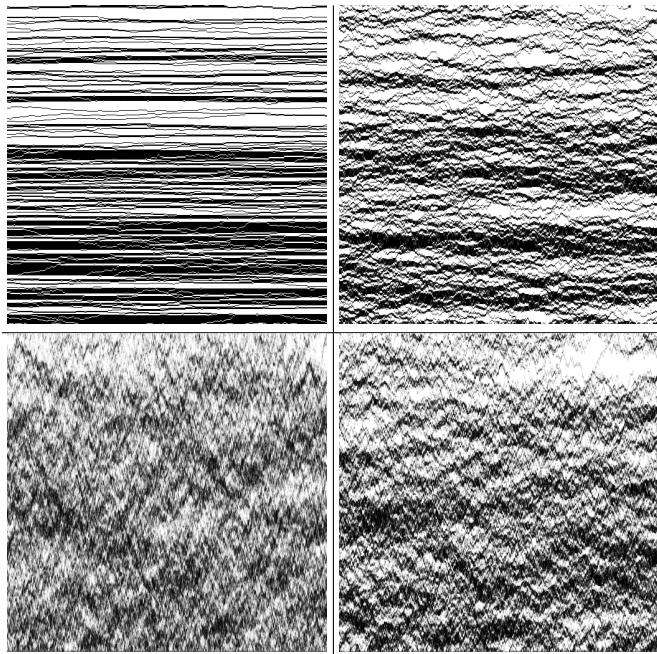

FIG. 4. As the logarithmic plot in Fig. 3, but over a much wider range of λ values. Notice how the data series from the two Monte-Carlo methods broaden and flatten as λ becomes very small; this is because of poor statistics due to the low flow rate.

B. Particle Motion During Flow

It is instructive to get an overview of how the particles move during flow. Fig. 5 show a plot of the flow structure in the slow-flow regime. In very short time averages the "striped" pattern indicates separation into dense and sparse regions, with an overall concentration gradient arising from the relative size of such regions. Particle/vacancy diffusion through the empty/full regions can be seen. As the averages are taken over longer times the blocks themselves appear to diffuse. Averaged over the entire simulation (not shown) the averaging simply gives a smooth density gradient.
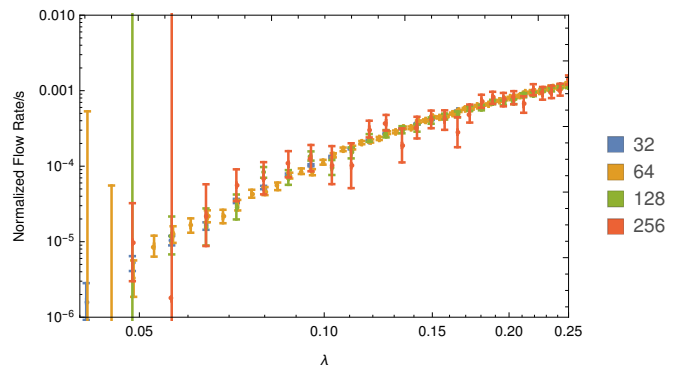

FIG. 6. The system size dependence of the normalized flow rate as a function of λ, computed using the KMC method. These calculations all have boundary conditions $(0.75, 0.25)$, and the flow rate has been normalized via multiplication by the system size (displayed on legend). Size 64 systems are a good compromise in terms of size and accuracy for a given amount of computational time.

FIG. 5. Indicative spacetime flow pattern for sticky free-flow $\left[\lambda = \frac{3}{20}, (\rho_0, \rho_L) = (\frac{3}{4}, \frac{1}{4})\right]$; other combinations shown in the supplementary materials. Time runs along the x-axis, space (1 pixel=1 site) along the y-axis, with grayscale tone (black being empty, white being full) illustrating average site occupation over (clockwise from top left) $\frac{1}{32}$, 1, 8 and 32 Gillespie steps per site respectively.

Interesting structure is visible, the dynamics appearing as a random walk with some tendency for particles to clump; over longer timescales the diffusive behavior is more evident, with a textured structure suggesting characteristic velocity of particles or vacancies through emergent correlated clumps. Additional plots can be found in the supplementary materials.

C. Transition in flow character

Fig. 4 shows how the current varies with stickiness at fixed driving for a very broad range of λ. At high λ the

rate is simply proportional to λ for any forcing. This result is far from trivial - it means that the overall flow is determined by the *faster* rate (λ), not the slower rate (1). That the MFT averages over the two is unsurprising (Eq. 12), but for the simulation to avoid having a "rate limiting step" requires the system to fill to sufficient density that there are always particles in contact to repel one another.

When $\lambda = \lambda_c \sim 0.2$ the simulations show a transition to a different behavior, with higher or lower λ_c depending on the boundary conditions and the strength of the driving force. The current and its fluctuation remains finite, but there a distinctive peak in the particle density fluctuation $< (\rho - \bar{\rho})^2$ (Fig. 7). The width of the peak is independent of the system size which suggests a continuous phase transition from the free flowing to the "stuck" regime.

Figs. 3 and 4 reveal that in the $(0.3, 0.1)$ and $(0.75, 0.25)$ boundary configurations the current switches from being $\mathcal{O}(\lambda)$ at high λ to being $\mathcal{O}(\lambda^k)$, $k \sim 4$ for low λ. In the high-density case, with boundary densities $(0.9, 0.7)$, the current actually starts flowing backwards for low λ in the transition rate matrix calculation. Therefore, we propose that the peak in the density fluctuation and the odd behavior in the current suggest the existence of a nonequilibrium phase transition in the SPM.

D. Effective diffusion constant

Using boundary conditions $(\rho_0, \rho_L) = (\rho_M + \frac{1}{2}\delta\rho, \rho_M - \frac{1}{2}\delta\rho)$ we demonstrate the dependence of current on boundary density difference and λ (Fig. 10). This shows that the transition to the stuck phase is suppressed by stronger driving forces (large $|\delta\rho|$)

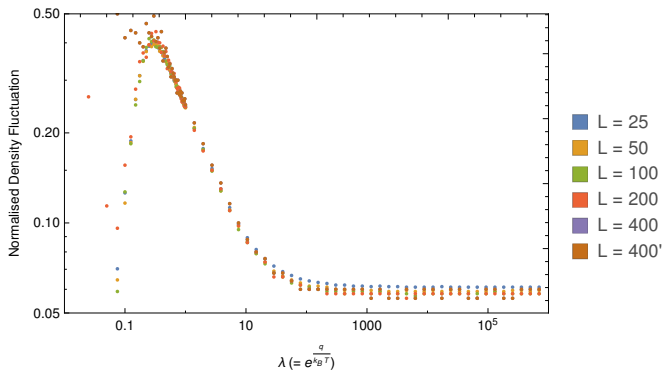We use the limit of small $\delta\rho$ to calculate the effective

FIG. 7. The scaling of the normalized fluctuation in the overall system density with system size, as a function of λ and with boundary conditions $(0.6, 0.4)$. This was computed using the traditional Metropolis-Hastings method. The normalization was achieved by multiplying by the system size, L. The great deal of coherence between these results regardless of size suggests that the fluctuation is of the normal Gaussian type, and not the kind of anomalously-scaling fluctuation associated with equilibrium phase transitions.

diffusion constant (Fig. 11). This is normalized to 1 in the case of $\lambda = 1$, which is just SEP. The $\rho_M = 0$ limit corresponds to free flow of particles, so the diffusion constant here does to 1. Similarly the $\rho_M = 1$ limit is flow of vacancies, so $D \to \lambda$. One might expect a monotonic variation between these limits, but surprisingly the simulations show that there is always an extremal value for D close to $\rho_M = 2/3$: this is a minimum for $\lambda < 1$ and a maximum for $\lambda > 1$

E. Self-organized density

We calculated the time-averaged total number of particles in the system by updating a histogram of particle numbers as the simulation progresses. In each of our calculations, we make the initial configuration by randomly filling the system with particles and vacancies in such a way that the initial density should be $\frac{1}{2}(\rho_0 + \rho_L)$, and then run the system for a sufficient number of equilibration steps to destroy any initial transients.

In SEP, $(\lambda = 1)$ the density varies linearly across the system from ρ_0 to ρ_L, as one expects for a diffusion process. However, for sticky particles, $\lambda < 1$, the density rises sharply near to the boundary, then has a linear profile about a value higher than ρ_M (Fig. 8). One might view this as particles being sucked into the system to lower their Hamiltonian Energy, but such a notion can be dismissed since the internal density *also rises for repelling particles*, $\lambda > 1$. The asymptotic values for the bulk density at high and low λ appear to be 1 and $\frac{2}{3}$ respectively, regardless of the mean boundary density ρ_M (see Fig. 9).
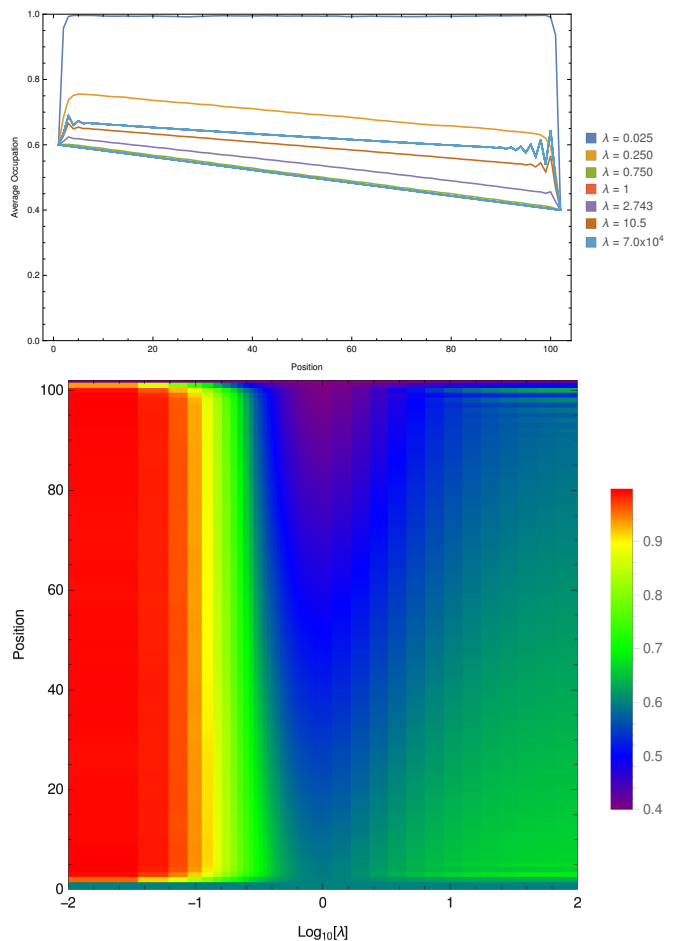

FIG. 8. The variation of the time-averaged density profile with respect to λ. The top panel shows this profile for a selection of values for λ in a system of size 100, with boundary conditions $(0.6, 0.4)$; the bottom panel displays this variation in the form of a colored density plot. Again, we have used the traditional Metropolis-Hastings method for these calculations. The oscillatory behavior near the boundary is a robust feature of the profile at high λ.

F. Review of the simulations

Simulation of the sticky particle model reveals a number of curious and unexpected features which have no equivalent in either SEP or the 1D Ising model.

- A transition in the dependence of the current on λ from $\propto \lambda$ to $\propto \lambda^4$.

- The mean density of the system has complicated variation with λ.

- The effective diffusion constant has an extremal value at intermediate boundary density.

To get further understanding of these behaviors, we tackle the system analytically, using mean field theory and transition rate matrices.
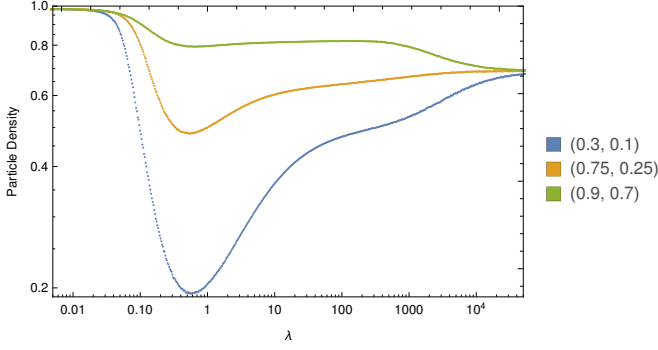
FIG. 9. The overall average density of a system of size 64, computed using KMC, with boundary conditions as specified in the plot. Notice how the density converges to 1 and $\sim \frac{2}{3}$ for extreme low and high λ respectively.

V. MEAN FIELD THEORY FOR FLOW

Let the spacing between lattice sites be a, let τ_0 be the free-particle hopping timescale, and the time-averaged (or ensemble-averaged, assuming ergodicity) occupation probability of the ith lattice site be ρ_i. We will introduce $\zeta = 1 - \lambda$ here for convenience.

A. Lattice Mean Field Theory

Let the ensemble-averaged occupation probability of the ith site at time t be $\rho_i(t)$. In the mean-field approximation this is assumed to be independent of $\rho_j(t)$ for $j \neq i$ at equal times. Therefore, if the ith site is occupied, then the rate at which it empties is the sum of contributions from the four permutations of the $(i+1)^{\text{th}}$ and $(i-1)^{\text{th}}$ occupancy:

$$
\begin{aligned}
&\frac{1}{\tau_0}(1 - \rho_{i-1})\left[(1 - \rho_{i+1}) + \lambda \rho_{i+1}\right] \\
&+ \frac{1}{\tau_0}(1 - \rho_{i+1})\left[(1 - \rho_{i-1}) + \lambda \rho_{i-1}\right].
\end{aligned}
\tag{7}
$$

Similarly, if the $(i)^{\text{th}}$ site is unoccupied, it fills with rate which depends on the occupation probability of the neighbours, and whether they are stuck to the $(i+2)^{\text{th}}$ and $(i-2)^{\text{th}}$ sites respectively. Therefore, an unoccupied i^{th} site fills with rate

$$
\frac{1}{\tau_0}\left\{\rho_{i+1}\left[\lambda\rho_{i+2} + (1 - \rho_{i+2})\right] + \rho_{i-1}\left[\lambda\rho_{i-2} + (1 - \rho_{i-2})\right]\right\}.
\tag{8}
$$

If we now multiply the filling/emptying rates of site i by the probability of being empty/full respectively, we

obtain the final equation for the site occupation

$$
\begin{aligned}
\tau_0 \frac{\partial \rho_i}{\partial t} = &(1 - \rho_i)\left[(1 - \zeta\rho_{i-2})\rho_{i-1} + (1 - \zeta\rho_{i+2})\rho_{i+1}\right] \\
&- \rho_i\left[2\zeta\rho_{i-1}\rho_{i+1} - (3 - \zeta)(\rho_{i-1} + \rho_{i+1}) + 2\right].
\end{aligned}
\tag{9}
$$

B. Diffusion Equation: MFT Continuum Limit

To obtain the continuum limit of the MFT we substitute $\rho_i(t) \to \rho(x,t)$, $\rho_{i+m}(t) \to \rho(x + am, t)$ into Eq. 9. Then, using a Taylor expansion around x for small a, neglecting terms of $\mathcal{O}(a^4)$, and collecting terms we find that

$$
\begin{aligned}
\tau_0 \frac{\partial \rho}{\partial t} = &a^2\left[1 - \zeta\rho(4 - 3\rho)\right]\frac{\partial^2 \rho}{\partial x^2} \\
&+ 2a^2\zeta(3\rho - 2)\left(\frac{\partial \rho}{\partial x}\right)^2 + \mathcal{O}(a^4),
\end{aligned}
\tag{10}
$$

which can be factorized into the more familiar form of a continuity equation

$$
\frac{\partial \rho}{\partial t} = \frac{a^2}{\tau_0}\frac{\partial}{\partial x}\left\{\left[1 - \zeta\rho(4 - 3\rho)\right]\frac{\partial \rho}{\partial x}\right\},
\tag{11}
$$

having dropped the higher-order terms. From this we can identify the flow $J(x)$ as the term in the curly brackets, and define a mean field diffusion constant (see Fig.11):

$$
D_{MFT}(\zeta, \rho) = \frac{a^2}{\tau_0}\left[1 - \zeta\rho(4 - 3\rho)\right]
\tag{12}
$$

We note that the MFT diffusion constant can become negative. The density at which this occurs is given by finding the roots ρ_c of the RHS of Eq. 12:

$$
\rho_c = \frac{2}{3} \pm \frac{1}{3}\sqrt{(4 - 3/\zeta)}.
\tag{13}
$$

The possible values for ρ_c are only real (and therefore physically possible) for $\zeta < 0.75$. So in the limit of very sticky particles ($\lambda < 0.25$) the MFT predicts a transition between forward and backwards diffusion at some densities.

C. Limiting Cases

In order to understand the implications of the MFT, let us consider some limits. As $\zeta \to 0$ (i.e. as the model becomes a simple exclusion model), $D \to \frac{a^2}{\tau_0}$. Likewise, in the dilute limit $\rho \to 0$, $D \to \frac{a^2}{\tau_0}$, reflecting the fact that it becomes a dilute lattice gas and therefore the interactions between particles become irrelevant as they never meet. Conversely, in the full limit $\rho \to 1$, $D \to \frac{\lambda a^2}{\tau_0}$; this is

because we now have a dilute gas of vacancies, which hop with rate $\frac{\lambda}{\tau_0}$.

One may observe that the MFT has a symmetry under $\rho \mapsto \frac{4}{3} - \rho$; thus, the dynamics should be symmetric under a density profile reflection around $\rho = \frac{2}{3}$. This is where D always attains its extremal value, $\frac{a^2}{\tau_0}\left[1 - \frac{4}{3}\zeta\right]$, hence for $\zeta > 3/4$ the diffusion coefficient becomes negative in regions with $\frac{2}{3} - \frac{\sqrt{\zeta(4\zeta-3)}}{3\zeta} < \rho < \frac{2}{3} + \frac{\sqrt{\zeta(4\zeta-3)}}{3\zeta}$.

Finally, it is possible to show that solutions to the continuum MFT containing domains with a negative diffusion coefficient are linearly unstable; thus, if we try to have a flow containing ρ for which $D(\rho) < 0$, the density of the medium should gravitate towards one of the two densities for which $D(\rho) \sim 0$. Instead of observing "backwards diffusion" we would see an extremely slow flow or no flow at all.

D. Steady State Flow

It is possible to solve the continuum MFT in a steady state on a finite domain, say $x \in (0, L)$. Steady state implies that there is no build-up of particles $\frac{\partial \rho}{\partial t} = 0$, so the flow is constant through the system.

Using the constant-flow requirement for continuity $J(x) = J_0 = \text{const.}$, and by integrating both sides of Eq. 11 with respect to x we find that

$$\int_{x_0}^x J(x')dx' = -\frac{a^2}{\tau_0}\int d\rho\left[1 - \zeta\rho(4 - 3\rho)\right] \quad (14)$$

$$(x - x_0)J_0 = -\frac{a^2}{\tau_0}\left[\rho + \zeta(\rho - 2)\rho^2\right]. \quad (15)$$

The density profile across the system is given by solving for $\rho(x)$. Since Eq.15 is cubic, the solution for density $\rho(x)$ is non-unique for cases of high ζ. Thus in the limit of high stickiness, the MFT is unable to make a unique prediction for the density. Furthermore, except in the SEP case $\zeta = 0$, the density will not vary linearly across the system.

E. Dirichlet Boundary Conditions

The constants x_0 and J_0 are the boundary conditions for the flow, but they need not correspond to a physically-realizable situation. For driven systems it is more convenient to consider fixing the density at each end.

If we impose such Dirichlet boundary conditions on this system, say $\rho(0) = \rho_0$ and $\rho(L) = \rho_L$, we find that

$$J_0 = \frac{a^2}{L\tau_0}\left[\rho_0 - \rho_L + \zeta\left(\rho_0\left[\rho_0^2 - 2\right] - \rho_L\left[\rho_L^2 - 2\right]\right)\right]. \quad (16)$$

This equation can be used for direct comparison with the simulations (Fig. 10 and Fig. 11). In general, the agreement is good, except for the region where the MFT predicts negative flow.

F. Interpretation of MFT

The mean field theory enables us to predict flow behavior of the MFT. It recovers well-known limiting cases such as SEP ($\lambda = 0$), however at high stickiness ($\lambda < 0.25$) it predicts its own demise, with unphysical negative diffusion constants and by having multiple solutions for the density at some positions in the system, meaning that the MFT does not give a unique density profile. This breakdown of the MFT corresponds to the transition to slow flow observed in the simulation.

In some conditions MFT predicts densities greater than 1. One might guess that when the MFT offers two possible values for the density, it will correspond to a phase separation in the actual system. Furthermore, the MFT prediction of a maximum diffusion constant at a density of $\rho = 2/3$ suggests that this value of ρ might be favoured for strongly driven flows.

A curious feature of the MFT diffusion (Fig. 11) is that for fixed stickiness there are *two possible densities* giving the same diffusion constant. Thus it is possible to have a steady state flow with phase separation into regions of high and low density. This echoes the situation seen in short time-averages of the simulation (Fig.5) where blocks of high and low density are evident, as well as the oscillatory behavior near the boundaries at high λ (Fig. 8).

Regarding the phase transition, we should note that we only have an MFT prediction for the flow rate as a function of λ, since $\rho(x)$ stops being unique when λ drops below $\frac{1}{4}$, and so the MFT lacks predictive power. For low-stickiness, when $\lambda > \frac{1}{4}$, the MFT is in very good agreement with the simulations, and this continues as λ stretches into the thousands, where the mean flow varies as $\mathcal{O}(\lambda^1)$.

The MFT prediction for the mean flow is again a good fit until λ becomes sufficiently small, when the simulation show no evidence of negative diffusion; rather the flow becomes critically slow for very sticky particles. The higher moments of the simulated flow (e.g. variance) do not show peaks, indicating that hard transitions are not occurring. Finally, the simulated density is very close to the average of the boundary densities until λ drops below $1/4$, at which point the system fills.

Continuing to specify the boundary densities to be $(\rho_0, \rho_L) = (\rho_M + \frac{1}{2}\delta\rho, \rho_M - \frac{1}{2}\delta\rho)$ for some given ρ_M, we can keep $\delta\rho$ relatively small, so that J varies approximately linearly with $\delta\rho$; thus if we calculate J for a series of small $\delta\rho$, we can perform linear regression to find $D_{\text{Eff}} = \frac{\partial J}{\partial \delta\rho}\big|_{\delta\rho=0}$, the effective diffusion coefficient. Computing this for different (ρ_M, λ) combinations yields results that can be compared with Eq. 16.
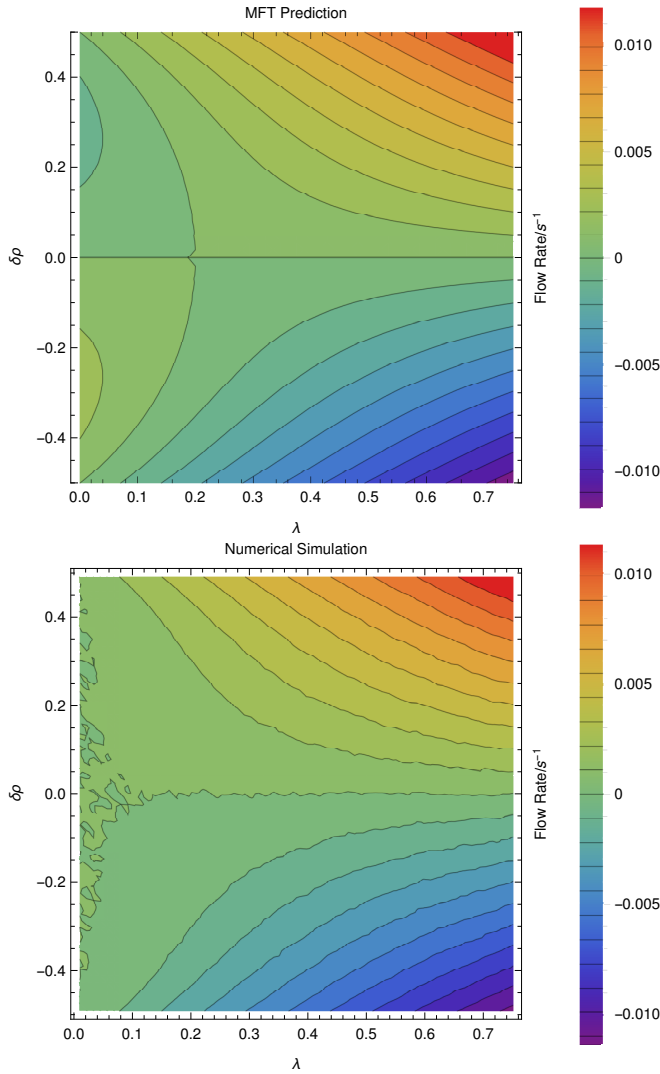
FIG. 10. Flow rate mean observed when varying the difference $\delta\rho$ between the boundary concentrations $(\rho_0, \rho_L) = (\rho_M + \frac{1}{2}\delta\rho, \rho_M - \frac{1}{2}\delta\rho)$ and λ (The top panel is the MFT prediction for the flow rate, whilst bottom shows the observed mean flow rate). We chose $\rho_M = \frac{1}{2}$, as this gives us the biggest range of $\delta\rho$ to investigate. These calculations were performed with the same run parameters (system length etc) as described in Fig. 11. The MFT prediction (top) shows a region of negative flow - this occurs at $\zeta > \frac{4}{5}$ ($\lambda < 0.2$) for the weakest driving force, with additional stickiness required when the driving force increases. The simulation exhibits close to zero flow in that region (bottom). Away from this region, the MFT and the simulation are in good agreement.

VI. DISCUSSION AND CONCLUSIONS

The sticky particle model is the combination of the Ising model with symmetric exclusion process. It arguably represents the simplest possible flow model for interacting particles is a homogeneous medium.

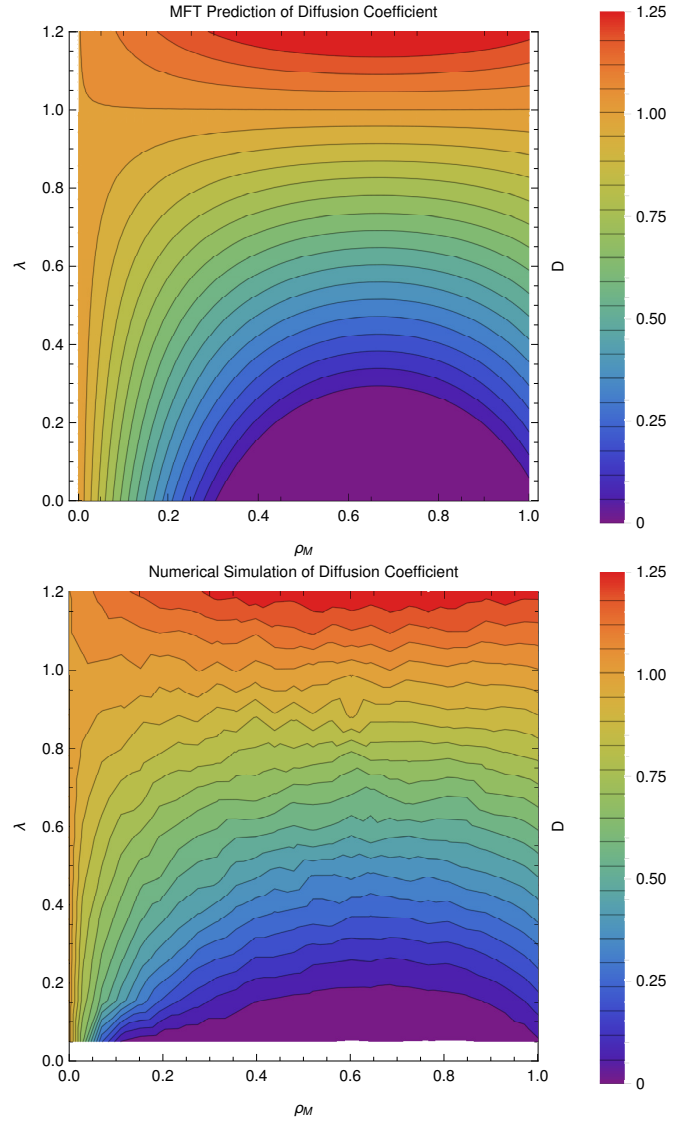Although only the particles exhibit stickiness, the an-

FIG. 11. Comparison of effective diffusion coefficient D in the MFT (top) and in direct simulation (bottom) as a function of density and stickiness. The white region is where the MFT gives negative diffusion. The simulations used 124 sites averaged over $\sim 10^9$ steps at each of $12 \times 24 \times 16$ ($\lambda, \rho_M, \delta\rho$) combinations. Full details in the supplementary materials.

alytics suggest a symmetry between vacancy-type and particle-type flow at density of $\frac{2}{3}$, which is observed in the simulation. The flow exhibits a foamy pattern with intermediate time-and-space correlations. The continuum solution MFT is a good predictor of the bulk flow behavior of the SPM. The negative diffusion constant found in MFT at high stickiness indicates that the assumption of homogeneous density break down: thus the MFT predicts its own demise, and this agrees well with our numerics.

Above a certain level of stickiness, the model exhibits a nonequilibrium phase transition to a slow-flowing phase. The required stickiness for the transition is dependent on

the strength of the driving force - a strongly driven system inhibits the flow. Mean field analysis, together with visualization of the flowing system, suggest that the transition comes when the density becomes inhomogeneous.

A number of questions remain open. Is there a physical principle which determines the density? Why does the strongly repelling system produce a density with maximum flow? Can one derive the λ^4 dependence of the slow-flow?

[1] V. Belitsky and G. M. Schütz, Journal of Statistical Mechanics: Theory and Experiment **2011**, P07007 (2011).

[2] M. Mobilia, I. T. Georgiev, and U. C. Täuber, Journal of Statistical Physics **128**, 447 (2007).

[3] B. Tegner, L. Zhu, C. Siemers, K. Saksl, and G. Ackland, Journal of alloys and compounds **643**, 100 (2015).

[4] L. Zhu, Q.-M. Hu, R. Yang, and G. Ackland, Journal of Physical Chemistry C **116**, 24201 (2012).

[5] B. E. Deal and A. S. Grove, Journal of Applied Physics **36**, 3770 (1965), https://doi.org/10.1063/1.1713945.

[6] N. Cabrera and N. F. Mott, Reports on Progress in Physics **12**, 163 (1949).

[7] S. Buzzaccaro, R. Rusconi, and R. Piazza, Phys. Rev. Lett. **99**, 098301 (2007).

[8] A. J. C. Ladd, M. E. Colvin, and D. Frenkel, Phys. Rev. Lett. **60**, 975 (1988).

[9] T. M. Liggett, *Interacting particle systems* (Springer-Verlag, Berlin, 1985).

[10] E. Ben-Naim, S. Y. Chen, G. D. Doolen, and S. Redner, Phys. Rev. Lett. **83**, 4069 (1999).

[11] S. F. Shandarin and Y. B. Zeldovich, Rev. Mod. Phys. **61**, 185 (1989).

[12] L. Frachebourg, Phys. Rev. Lett. **82**, 1502 (1999).

[13] L. Frachebourg, P. A. Martin, and J. Piasecki, Physica A Statistical Mechanics and its Applications **279**, 69 (2000), cond-mat/9911346.

[14] V. V. Obukhovsky, A. M. Kutsyk, V. V. Nikonova, and O. O. Ilchenko, Phys. Rev. E **95**, 022133 (2017).

[15] N. V. Gorokhova and O. E. Melnik, Fluid Dynamics **45**, 679 (2010).

[16] M. Kardar, G. Parisi, and Y.-C. Zhang, Phys. Rev. Lett. **56**, 889 (1986).

[17] J. Krug and H. Spohn, Phys. Rev. A **38**, 4271 (1988).

[18] T. Sasamoto and H. Spohn, Phys. Rev. Lett. **104**, 230602 (2010).

[19] K. E. P. Sugden and M. R. Evans, Journal of Statistical Mechanics: Theory and Experiment **2007**, P11013 (2007).

[20] M. Kollmann, Phys. Rev. Lett. **90**, 180602 (2003).

[21] B. Lin, M. Meron, B. Cui, S. A. Rice, and H. Diamant, Phys. Rev. Lett. **94**, 216001 (2005).

[22] C. Hegde, S. Sabhapandit, and A. Dhar, Phys. Rev. Lett. **113**, 120601 (2014).

[23] P. L. Krapivsky, K. Mallick, and T. Sadhu, Phys. Rev. Lett. **113**, 078101 (2014).

[24] T. Imamura, K. Mallick, and T. Sasamoto, Phys. Rev. Lett. **118**, 160601 (2017).

[25] S. Katz, J. L. Lebowitz, and H. Spohn, Journal of Statistical Physics **34**, 497 (1984).

[26] R. K. P. Zia, Journal of Statistical Physics **138**, 20 (2010).

[27] Y. Kafri, E. Levine, D. Mukamel, G. M. Schütz, and R. D. Willmann, Phys. Rev. E **68**, 035101 (2003).

[28] K. Kawasaki, Phys. Rev. **145**, 224 (1966).

[29] M. Leetmaa and N. V. Skorodumova, Computer Physics Communications **185**, 2340 (2014), arXiv:1405.1221 [physics.comp-ph].

[30] D. T. Gillespie, The Journal of Physical Chemistry **81**, 2340 (1977), http://dx.doi.org/10.1021/j100540a008.

[31] A. Bortz, M. Kalos, and J. Lebowitz, Journal of Computational Physics **17**, 10 (1975).

[32] A. Prados, J. J. Brey, and B. Sánchez-Rey, Journal of Statistical Physics **89**, 709 (1997).

[33] J. Hellier, (2018), 10.5281/zenodo.1162818.

[34] C. P. Robert, "The metropolis-hastings algorithm," in *Wiley StatsRef: Statistics Reference Online* (American Cancer Society, 2015) pp. 1–15.